7-5-2018

Phase Modulation of (1T-2H)-MoSe2/TiC-C Shell/Core Arrays via Nitrogen Doping for Highly Efficient Hydrogen Evolution Reaction

Shengjue Deng
Zhejiang University

Fan Yang
Hainan University

Qinghua Zhang
Chinese Academy of Sciences

Yu Zhong
Zhejiang University

Yinxiang Zeng
Sun Yat-sen University

See next page for additional authors

Phase Modulation of (1T-2H)-MoSe2/TiC-C Shell/Core Arrays via Nitrogen Doping for Highly Efficient Hydrogen Evolution Reaction

Abstract
Tailoring molybdenum selenide electrocatalysts with tunable phase and morphology is of great importance for advancement of hydrogen evolution reaction (HER). In this work, phase- and morphology-modulated N-doped MoSe2/TiC-C shell/core arrays through a facile hydrothermal and postannealing treatment strategy are reported. Highly conductive TiC-C nanorod arrays serve as the backbone for MoSe2 nanosheets to form high-quality MoSe2/TiC-C shell/core arrays. Impressively, continuous phase modulation of MoSe2 is realized on the MoSe2/TiC-C arrays. Except for the pure 1T-MoSe2 and 2H-MoSe2, mixed (1T-2H)-MoSe2 nanosheets are achieved in the N-MoSe2 by N doping and demonstrated by spherical aberration electron microscope. Plausible mechanism of phase transformation and different doping sites of N atom are proposed via theoretical calculation. The much smaller energy barrier, longer H□Se bond length, and diminished bandgap endow N-MoSe2/TiC-C arrays with substantially superior HER performance compared to 1T and 2H phase counterparts. Impressively, the designed N-MoSe2/TiC-C arrays exhibit a low overpotential of 137 mV at a large current density of 100 mA cm−2, and a small Tafel slope of 32 mV dec−1. Our results pave the way to unravel the enhancement mechanism of HER on 2D transition metal dichalcogenides by N doping.

Keywords
core/shell arrays, hydrogen evolution reaction, molybdenum selenide, nitrogen doping, phase modulation

Disciplines
Engineering Physics

Authors
Shengjue Deng, Fan Yang, Qinghua Zhang, Yu Zhong, Yinxiang Zeng, Shiwei Lin, Xiuli Wang, Xihong Lu, Cai-Zhuang Wang, Lin Gu, Xinhui Xia, and Jiangping Tu

DOI: 10.1002/ ((please add manuscript number))

Article type: Communication

Phase Modulation of (1T-2H)-$MoSe_2$/TiC-C Shell/Core Arrays via Nitrogen Doping for Highly Efficient Hydrogen Evolution Reaction

Shengjue Deng[‡], Fan Yang[‡], Qinghua Zhang, Yu Zhong, Yinxiang Zeng, Shiwei Lin, Xiuli Wang, Xihong Lu*, Cai-Zhuang Wang, Lin Gu, Xinhui Xia* and Jiangping Tu*

S. J. Deng, Y. Zhong, Prof. X. L. Wang, Prof. X. H. Xia, Prof. J. P. Tu

State Key Laboratory of Silicon Materials,

Key Laboratory of Advanced Materials and Applications for Batteries of Zhejiang Province, and Department of Materials Science and Engineering,

Zhejiang University,

Hangzhou 310027, P. R. China.

E-mail: helloxxh@zju.edu.cn

F. Yang, Prof. S. W. Lin

State Key Laboratory of Marine Resource Utilization in South China Sea, Hainan University, Haikou 570228, P. R. China

E-mail: linsw@hainu.edu.cn

Prof. Q. H. Zhang, Prof. L. Gu

Institute of Physics, Chinese Academy of Sciences

Y. X. Zeng, Prof. X. H. Lu

MOE of the Key Laboratory of Bioinorganic and Synthetic Chemistry, KLGHEI of Environment and Energy Chemistry, School of Chemistry,

Sun Yat-Sen University,

Guangzhou 510275, China.

E-mail: luxh6@mail.sysu.edu.cn

Prof. C. Z. Wang

Ames Laboratory-U. S. Department of Energy, and Department of Physics and Astronomy, Iowa State University, Ames, IA 50011, USA

‡ S. Deng and F. Yang contributed equally to this work

* Address correspondence to helloxxh@zju.edu.cn (X. H. Xia), linsw@hainu.edu.cn (S. W. Lin), and luxh6@mail.sysu.edu.cn (X. H. Lu)

Keywords: Molybdenum selenide; Nitrogen doping; Phase modulation; Hydrogen evolution reaction; Core/shell arrays

Abstract: Tailoring molybdenum selenide electrocatalysts with tunable phase and morphology is of great importance for advancement of hydrogen evolution reaction (HER). In this work, we report phase- and morphology-modulated N-doped $MoSe_2$/TiC-C shell/core arrays through a facile hydrothermal and post-annealing treatment strategy. Highly conductive TiC-C nanorod arrays serve as the backbone for $MoSe_2$ nanosheets to form high-quality $MoSe_2$/TiC-C shell/core arrays. Impressively, continuous phase modulation of $MoSe_2$ is realized on the $MoSe_2$/TiC-C arrays. Except for the pure 1T-$MoSe_2$ and 2H-$MoSe_2$, mixed (1T-2H)-$MoSe_2$ nanosheets are achieved in the N-$MoSe_2$ by N doping and demonstrated by spherical aberration electron microscope. Plausible mechanism of phase transformation and different doping sites of N atom are proposed via theoretical calculation. The much smaller energy barrier, longer H-Se bond length and diminished bandgap endow N-$MoSe_2$/TiC-C arrays with substantially superior HER performance compared to 1T and 2H phase counterparts. Impressively, the designed N-$MoSe_2$/TiC-C arrays exhibit a low overpotential of 137 mV at a large current density of 100 mA cm^{-2}, and a small Tafel slope of 32 mV Dec^{-1}. Our results pave the way to unravel the enhancement mechanism of HER on 2D transition metal dichalcogenides (TMDs) by N doping.

1. Introduction.

Interest in hydrogen as a way of delivering energy services has been growing in recent years in response to heightening concerns about the environmental impact of energy use and worries about the security of fossil-fuel supplies.[1-4] Currently, hydrogen is widely produced by steam reforming of fossil fuels (e.g., methane),[5] but this process causes emissions of carbon dioxide and airborne pollutants. Alternatively, carbon-free water electrolysis to generate environment-friendly and renewable hydrogen via electrochemical hydrogen evolution reaction (HER) has attracted ever-increasing attention.[6, 7] It is well accepted that the HER performance is closely bound up with the electrocatalysts. Noble metals (such as Pt and Pt-based alloys) are currently deemed to be the most promising electrocatalysts for HER with low overpotentials and Tafel slopes,[8-10] but their practical application is severely hindered by high cost, scarcity and compromised long-term stability. To this end, it is highly desirable to develop cost-effective and efficient HER electrocatalysts.

Of the explored candidates, molybdenum selenide ($MoSe_2$) has been one of the hotspot research subjects due to its superior stability, easy processing, and good HER performance.[11] It is demonstrated that the HER performance of $MoSe_2$ is closely linked with its phase. It is known that $MoSe_2$ has two active phases[12]: 2H phase with trigonal prismatic lattice and 1T phase with trigonal lattice (octahedral coordination).[13] The 1T-$MoSe_2$ exhibits

metallic properties with better HER performance, while the 2H-$MoSe_2$ is a p-type semiconductor with relatively lower electronic conductivity & catalytic activity.[14] Meanwhile, it is noteworthy that the 2H-$MoSe_2$ is a steady state, while the 1T-$MoSe_2$ is a metastable state and can be easily converted into 2H-$MoSe_2$. To obtain stable 1T-$MoSe_2$ nanostructures for HER performance, two main strategies have been proposed. The first route is to directly synthesize 1T-$MoSe_2$ nanostructures, but just only a few works reported. Jiang et al.[15] and Yin et al.[16] reported solvothermal/hydrothermal methods to prepare 1T-$MoSe_2$ nanosheets with enhanced HER performance (Tafel slope of 78 mV dec^{-1} and 52 mV dec^{-1}, respectively). Nevertheless, their structural stability and electronic conductivity are still not satisfactory. In addition, without support of conductive matrix, the large-current HER performance of the above 1T-$MoSe_2$ nanosheets powder are greatly undermined. The second route is to introduce 1T-$MoSe_2$ into 2H-$MoSe_2$ host to create mixed stable (1T-2H)-$MoSe_2$. For example, Qu et al.[17] adopted plasma-assisted selenization process to produce Mo/(1T-2H)-$MoSe_2$ core/shell arrays with Tafel slope of ~35 mV dec^{-1}. But the plasma-assisted selenization process requires sophisticated equipment and high cost. Recently, our group[11] successfully employed an annealing process to form (1T-2H)-$MoSe_2$ on graphene with Tafel slope of 49 mV dec^{-1}. This (1T-2H)-$MoSe_2$/graphene composite showed stable structure, good cycling life and enhanced HER performance as compared to the pure

2H-$MoSe_2$ counterpart. However, there are still some underlying problems such as the unknown phase modulation mechanism and undesirable overpotential at large current density. Additionally, it still a challenge to realize modulation between different phases (1T, 2H and 1T-2H) of $MoSe_2$ and unravel the reason of their performance difference of HER.

Catalytic current at a specific potential is another indicator to illustrate the HER performance. Under the same conduction, higher current density implies better HER efficiency. To date, most of the works adopted the current density of 10 mA cm^{-2} as the benchmark to compare the HER performance,[18, 19] and there is no work on HER comparison of $MoSe_2$ at larger current density such as100 mA cm^{-2}. To realize large current HER, apart from the phase engineering, morphology engineering is indispensable.[13, 20-22] Power form is usually not suitable for large current HER due to the use of insulating binders and detach from substrate arising from bubble-striking effect. Therefore, stable and highly conductive backbones (e.g., reduced graphene oxide,[23] carbon fibre,[24] carbon nanotubes[25] and Mo[17]) are needed to couple with $MoSe_2$ to enhance the electron transfer and mechanical stability. Currently, CVD-derived TiC-C arrays are becoming the new pet as the conductive matrix for electrochemical application (TiC-C/Si,[26] TiC-C/Li,[27] and so on) due to their excellent structural/chemical stability, high electrical conductivity (10^5 S/m) and strong mechanical stability. Consequently, the TiC-C arrays are excellent skeletons for large-current HER.

Nevertheless, to date, there is no report on rational combination between $MoSe_2$ and TiC-C skeleton. Therefore, it would be very interesting to explore the directional growth of $MoSe_2$ with different phases on the TiC-C skeleton to form high-quality binder-free electrocatalysts for advanced HER.

In this wok, combining the phase & morphology engineering strategies together, we design high-quality N doped $MoSe_2$/TiC-C shell/core arrays with exceptional HER activity. Starting from hydrothermal-synthesized 1T-$MoSe_2$/TiC-C arrays, we realize the phase modulation of $MoSe_2$ from 1T phase to 2H phase and mixed 1T-2H phase via a facile hydrothermal plus annealing process and demonstrated by spherical aberration electron microscope. Finally, interconnected (1T-2H)-$MoSe_2$ nanosheet shell obtained by N doping (designated as N-$MoSe_2$) is intimately anchored on the highly conductive TiC-C nanowire core forming self-supported HER electrocatalysts. The DFT calculation conducted on phase transformation and different doping sites reveal that N doping not only decreases the band gap of $MoSe_2$, but also reduces the energy barrier promoting easier phase transition from 2H to 1T, which provides useful insights to further understand the enhancement mechanism of HER by N doping. Benefiting from highly conductive support of TiC-C arrays, improved conductivity, richer catalytic active sites, and lower desorption energy, the fabricated N-$MoSe_2$/TiC-C arrays exhibit the best HER performance both at routine current density of 10 mA cm^{-2} and

large current density of 100 mA cm^{-2}, with the lowest overpotentials and smallest Tafel slopes, better than other 1T-$MoSe_2$ and 2H-$MoSe_2$ counterparts. Our work provides useful insight to understand the enhancement mechanism of HER by N doping and offers new means for construction of advanced electrocatalysts for water electrolysis and beyond.

2. Results and discussion

The simplified schematic flow of synthesis process of N-$MoSe_2$/TiC-C arrays is illustrated in **Figure 1**a. First of all, the TiC-C arrays are prepared on the Ti_6Al_4V foil via a facile CVD method. As shown in **Figure 1**b-c, uniform TiC-C nanorods of ~300 nm in diameters grow vertically to the Ti_6Al_4V foil substrate forming array architecture. Moreover, the TiC-C nanorods individually grow with non-interference and leave lots of interspace of 1-3 μm forming arrays network. The shell/core structure of the TiC-C is clearly distinguished by transmission electron microscopy (TEM) images (**Figure S1**), which demonstrate that the TiC nanowire core of ~30 nm is homogeneously covered by carbon shell with thickness of about 130-150 nm (**Figure S1**a-b). Selected area electron diffraction (SAED) patterns show that the

TiC core is sing-crystalline in nature, while the carbon shell is amorphous (**Figure S1**b). The measured lattice fringe is about 0.22 nm, corresponding to the interplanar spacing of (002) planes of TiC phase (JCPDS 65-0242). No clear lattice fringe is noticed for the carbon shell, further confirming its amorphous nature (**Figure S1**c). Energy dispersive X-ray (EDS) mapping images (**Figure S1**d-f) confirm the existence and uniform distribution of C and Ti elements in TiC-C shell/core arrays. These unique structure characteristics endows the TiC-C arrays with high electronic conductivity, which is verified by four-point probe method with a small resistance of 1.6 mΩ/sq. This is very important for HER at large current density requiring fast transfer paths for electrons. After the hydrothermal (HT) process, wrinkled $MoSe_2$ nanosheets are homogeneously grown along the TiC-C nanorods to form 1T-$MoSe_2$/TiC-C arrays. Note that the whole surface of the TiC-C nanorod is completely decorated by interconnected ultrathin $MoSe_2$ nanosheets (**Figure 1**d-e), suggesting the successful deposition of $MoSe_2$ on TiC-C backbone forming shell/core arrays. The 1T-$MoSe_2$ can be converted into 2H-$MoSe_2$ after thermal treatment (TT) under argon atmosphere. Furthermore, the 2H-$MoSe_2$/TiC-C arrays can be further changed into (1T-2H)-$MoSe_2$/TiC-C arrays by N doping via NH_3 annealing (designated as N-$MoSe_2$/TiC-C). The N doping can modulate the phase of $MoSe_2$ and realize the co-existence of 1T and 2H phase in the $MoSe_2$ nanosheets. It is seen that both 2H-$MoSe_2$/TiC-C and N-$MoSe_2$/TiC-C arrays exhibit similar

morphologies to that of the 1T-$MoSe_2$/TiC-C arrays (**Figure 1**h-i and **1**k-l). The 3D porous networks are still well preserved and the diameters of arrays do not change much. The above results suggest that the NH_3 treatment will not obviously affect the morphology of products.

The phase evolution of $MoSe_2$/TiC-C arrays was monitored and supported by TEM-HRTEM and spherical aberration corrected transmission electron microscope (SACTEM) analysis in detail. TEM images (**Figure 2**a-c) indicate that, for all three samples, the TiC-C core is uniformly decorated by the cross-linked $MoSe_2$ nanosheets shell, forming high-quality shell/core structures. The diameters of the $MoSe_2$/TiC-C core/shell structures are about 700-800 nm. Moreover, the line-scan energy dispersive X-ray (EDX) spectra (**Figure S2**) shows the relative intensity of the C, Ti, Mo Se and N elements, further confirming the core/shell structure of N-$MoSe_2$/TiC-C. TEM images further verify that there is no noticeable change on morphology for all three samples. The lattice fringe evolution of $MoSe_2$ nanosheets at different stages is shown in HRTEM images (**Figure 2**a-c). Note that the interlayer distance of the 1T-$MoSe_2$ nanosheets is about 0.71 nm characteristic of the 1T-$MoSe_2$ phase.[11, 17, 28-30] This value decreases into 0.65 nm for the 2H-$MoSe_2$ nanosheets,[13, 24] and then increases up to 0.68 nm for the (1T-2T)-$MoSe_2$ nanosheets by N doping due to the co-existence of 1T and 2H phases. The above results suggest that the hydrothermal-synthesized 1T-phase $MoSe_2$ can be easily converted into 2H-phase due to the

effect of high temperature. With the introduction of N, partial 2H-phase could be converted into 1T-$MoSe_2$, because the N doping can trigger rearrangement of Se and Mo atoms to generate the final (1T-2H)-$MoSe_2$/TiC-C shell/core arrays, further supported by detailed HRTEM analysis. Notice that the 1T-$MoSe_2$ shows trigonal lattice structure (octahedral coordination) (**Figure 2**d and **2**g), different from the 2H-$MoSe_2$ with common honeycomb lattice (trigonal prismatic coordination) (**Figure 2**e and 2h).[11, 30] In addition, the measured lattice fringe of 2H-$MoSe_2$ is around 0.285 nm, larger than the 1T-$MoSe_2$ (0.276 nm) (**Figure 2**d-e), matching well with the (100) plane of $MoSe_2$ (JCPDS 29-0914). Impressively, both the lattice structures of 1T- and 2H-phases are clearly presented in N-$MoSe_2$/TiC-C arrays (**Figure 2**f and **2**i), indicating that the N doping can modulate the $MoSe_2$ phase and realize the co-existence of 1T-$MoSe_2$ and 2H-$MoSe_2$ in N-$MoSe_2$ nanosheets. In order to check the phase evolution, selected area electron diffraction (SAED) measurements were conducted (**Figure 2**j-l). The radii of diffraction rings of (100), (103), and (110) correspond to different lattice spacings. The 1T-$MoSe_2$ shows larger lattice spacing of (103) and (110) planes, but possesses smaller lattice spacing of (100) plane compared to 2H-$MoSe_2$. Remarkably, the lattice spacing of N-$MoSe_2$ is between 1T-$MoSe_2$ and 2H-$MoSe_2$, further demonstrating the formation of (1T-2H)-$MoSe_2$/TiC-C arrays, consistent with the results above.

X-ray diffraction (XRD), Raman and X-ray photoelectron spectroscopy (XPS) tests were also performed to investigate the phase and chemical composition of all samples. Typical XRD patterns of the TiC-C, 1T-$MoSe_2$/TiC-C, 2H-$MoSe_2$/TiC-C and N-$MoSe_2$/TiC-C samples are presented in **Figure S3**. Apart from the peaks of Ti_6Al_4V foil substrate, five diffraction peaks characteristic of TiC phase (JCPDS 65-0242) and one broad diffraction peak characteristic of amorphous carbon at 26° are detected in the TiC-C arrays. Except for the diffraction peaks of TiC-C backbone, the other peaks of the 1T-$MoSe_2$/TiC-C sample are in good agreement with 1T-phase $MoSe_2$, which has disappeared peak of (002) plane and strong (100) plane. As for the 2H-$MoSe_2$/TiC-C arrays, the typical diffraction peaks of (002) and (100) planes are clearly observed, and all diffraction peaks of $MoSe_2$ are indexed well with the 2H-phase $MoSe_2$ (JCPDS 77-1715). After N doping, typical diffraction peaks of TiC-C and $MoSe_2$ remain in the N-$MoSe_2$/TiC-C arrays, but noteworthy that the relative intensities of (100) and (002) peaks sharply decrease **(Figure S3**a). Furthermore, the (002) and (110) peaks shift leftward as compared to the 2H-$MoSe_2$/TiC-C sample.[17, 30] These results are consistent with the TEM analysis above. Another interesting finding is that there is no shift for the diffraction peaks of TiC-C in all three samples. The XRD results indicate that 1T-phase $MoSe_2$ can be easily changed into 2H-phase after heat treatment, and additionally, partial 2H-$MoSe_2$ can be converted into 1T-$MoSe_2$ after N doping. This finding is further

confirmed by Raman and XPS analyses. The characteristic Raman peaks of $MoSe_2$ in the 1T-$MoSe_2$/TiC-C are located at 237 and 285 cm^{-1} (**Figure S3**b), respectively, owing to the characteristic A_{1g} (out of plane) and E^1_{2g} (in plane) of $MoSe_2$.[6] Note that the characteristic peak of A_{1g} in the 2H-$MoSe_2$/TiC-C has a slight shift to a larger wavelength compared to the 1T-$MoSe_2$/TiC-C, implying the phase change from 1T-$MoSe_2$ to 2H-$MoSe_2$. Noticeably, FDHM (full depth at half maximum) of A_{1g} peak shown in the inset of **Figure S3**b increases as the phase change proceeds. Generally, the 1T-$MoSe_2$ shows weak Raman intensity, while the 2H phase has strong intensity. As for the N-$MoSe_2$/TiC-C, the intensity of FDHM is in the middle of 1T-$MoSe_2$/TiC-C and 2H-$MoSe_2$/TiC-C, suggesting the co-existence of 1T and 2H-$MoSe_2$.[17]

The XPS survey and high-resolution spectra of C, Ti, Se, Mo and N elements are depicted in **Figure S3** and **Figure S4**. In **Figure S3**c, two peaks at 228.3 eV (Mo 3d5/2) and 231.4 eV (Mo 3d3/2) characteristic of 1T-$MoSe_2$ are observed for the 1T-$MoSe_2$/TiC-C arrays.[31] After heat treatment in Ar, the Mo 3d spectra change and shift obviously. Two peaks located at 229 eV (Mo 3d5/2) and 232.1 eV (Mo 3d3/2) in the 2H-$MoSe_2$/TiC-C are indexed well with characteristic of 2H-$MoSe_2$. Upon doping, the Mo 3d5/2 and Mo 3d3/2 peak broadens can be deconvoluted to four peaks, corresponding to the co-existence of 1T and 2H-$MoSe_2$.[17] Such finding is also corroborated by Se 3d high-resolution spectra (**Figure S3**d). The Se 3d

spectrum mainly exhibits two typical peaks at 54.8 and 53.8 eV originating from Se ions for the 1T-$MoSe_2$/TiC-C arrays.[11, 17, 32] After annealing in argon, the peaks of 1T-phase vanish and two typical peaks of Se (55.4 and 54.5 eV) characteristic of 2H-$MoSe_2$ start to appear. Compared to other two samples, the peak intensity of 2H phase decreases and the 1T phase increases in the N-$MoSe_2$/TiC-C arrays. These results further confirm the co-existence of 1T and 2H-$MoSe_2$ in the N-$MoSe_2$/TiC-C sample. The presence of TiC is also confirmed by XPS result shown in **Figure S4**b-c. And the N doping is also verified by the peak at 398.5 eV (**Figure S4**d), which is due to the N-Mo bond.[33, 34] All these results mutually support each other and indicate the successful preparation of N-$MoSe_2$/TiC-C arrays.

To understand the phase change of $MoSe_2$ via N doping, we simulated the experimental results with the aid of in-depth theoretical study. We considered four possible doping sites in $MoSe_2$ (**Figure 3**a-b) based upon two $MoSe_2$ phases (**Figure 3**a-b): H_{in}, T_{Mo}, T_{Se} and N_{Se}. H_{in} stands for the interstitial site between the $MoSe_2$ layers and at the center of the six-membered ring formed by Se-Mo-Se atoms in both the upper and lower layers; T_{Mo} represents the interstitial site at the center of the four Mo atoms within a $MoSe_2$ layer; T_{Se} means the interstitial site at the center of the four Se atoms within a $MoSe_2$ layer; N_{Se} indicates that N replaces the position of Se atom. Since N source in the experiment is ammonia and N has negative valence, the substitution at the Mo site is unlikely and hence not considered.

According to simulated band structures and density-of-states (DOS) results (**Figure S5**), the electronic properties of 2H-$MoSe_2$ before and after N doping are quite different. The band gap of pure 2H-$MoSe_2$ is 1.22eV, while the structures with N-doped $MoSe_2$ in H_{in} and T_{Mo} site are quasi-metallic. The band gaps of the N-doped $MoSe_2$ in T_{Se} and N_{Se} configurations are 0.46 eV and 0.51 eV, respectively, much smaller than that of the pure 2H-$MoSe_2$. These results suggest that N doping can improve electronic conductivity and the effects from different doping sites are different. According to this observation, N doping can promote the phase transition from 2H-$MoSe_2$ to 1T-$MoSe_2$. In order to gain the insight into the transformation pathway and the effect of different N doping sites on the transformations, we have performed the first-principles calculations to study the pathway and energy barriers of the phase transition from 2H-$MoSe_2$ to 1T-$MoSe_2$. The calculation results show that the structure transformation involves stretching of unit cell along the **c**-axis and shuffling of the Se atoms in the unit cell. The transformation pathways and energy from 2H-$MoSe_2$ to 1T-$MoSe_2$ by N-doping in different sites obtained from our calculations are shown in **Figure S6**. Without N doping, the energy barrier would be 0.82 eV. After N-doping, the barrier is reduced to 0.77, 0.65, 0.58 and 0.25 for T_{Mo}, H_{in}, N_{Se}, and T_{Se} doping configurations, respectively (**Figure 3**c). The corresponding energy of simulated 1T-$MoSe_2$ phase is also lower than the direct transition with the help pf N doping. The energy of the obtained 1T

phase from direct conversion is 0.7 eV (**Figure 3**d and **S6**), but this relative energy is reduced to 0.38 eV, 0.39 eV, 0.21 eV, and 0.40 eV with N-doping at the H_{in}, T_{Mo}, T_{Se} and N_{Se} configurations, respectively (**Figure 4**d and S**6**). It is indicated that the phase transition from 2H-$MoSe_2$ to 1T-$MoSe_2$ is more favorable by N doping. When N doping at T_{Se} site, the phase transition barrier (0.25 eV) can be more easily overcome, and the formed 1T-$MoSe_2$ would be more stable than other doping sites. It is known that 2H-$MoSe_2$ belongs to $P\bar{6}m2$ space-group, where Mo and the surrounding Se form trigonal prisms. 1T-$MoSe_2$ belongs to $P\bar{3}m1$ space-group, where Mo and the surrounding Se are octahedrally coordinated. N doping in 2H-$MoSe_2$ changes the distribution of Se and distort the trigonal prism near the doping site, which induces stress in the crystal and causes the cell to stretch in the **c** direction. This can be more clearly seen in N doping at T_{Se}. When N doped at the center of the four Se atoms, it is easier to promote the distortion of Se and thus causing the phase transition.

The electrochemical HER performances (**Figure 4**) of all samples were detected by using a simple three-electrode setup in 0.5 M H_2SO_4 solution. The N-$MoSe_2$/TiC-C electrode displays the best HER performance with the smallest overpotential (-106 mV vs. RHE at 10 mA cm^{-2}) and excellent large-current HER performance of -137 mV at 100 mA cm^{-2}, better than the 1T-$MoSe_2$/TiC-C (-187 mV and -219 mV), 2H-$MoSe_2$/TiC-C (-240 mV and -365 mV) and TiC-C (no obvious HER activities) (**Figure 4**a), respectively. The unobvious HER

activity of TiC-C suggests that the TiC-C core mainly act as a highly conductive support for the $MoSe_2$ nanosheets. The superior catalytic performance in the N-$MoSe_2$/TiC-C electrode is attributed to the introduction of N dopant, further supported by the Tafel slope. According to classic theory[35, 36], Tafel slope can evaluate the limiting step based on three mechanisms of Volmer reaction (Tafel slope ≈120 mV dec^{-1}), Heyrovsky reaction (Tafel slope≈ 40 mV dec^{-1}) and Tafel reaction (Tafel slope ≈29 mV dec^{-1}). The most advanced and fastest HER process should be determined by Tafel reaction process of hydrogen recombination, which implies that smaller Tafel slope dictates faster HER process. In our study, the Tafel slopes of TiC-C, 1T-$MoSe_2$/TiC-C, 2H-$MoSe_2$/TiC-C and N-$MoSe_2$/TiC-C electrodes are 390, 42, 110 and 32 mV dec^{-1}, respectively (**Figure 4**b), suggesting N-$MoSe_2$ samples possess the fastest HER process. It indicated that the HER rate of N-$MoSe_2$/TiC-C arrays are determined by the Tafel reaction mechanism. The HER activities of our N-$MoSe_2$/TiC-C sample is not only superior to those reported Mo-based materials [14, 23, 37-39] (**Figure 4**c and **Table S1**), such as $MoSe_2$/Mo,[17] $MoSe_2$/CNTs[6] $MoSe_2$/C[40] MoS_2/SnO_2[41] and S-$MoSe_2$,[42] but even surprisingly higher than the Pt/C (Tafel slope ≈34 mV dec^{-1}).[6] To measure the electrochemical stability of our samples, the cycle durability on 1T-$MoSe_2$/TiC-C, 2H-$MoSe_2$/TiC-C and N-$MoSe_2$/TiC-C arrays was performed at 100 mA cm^{-2} for 4 h, respectively (**Figure 4**d). The N-$MoSe_2$/TiC-C electrode shows the highest potential retention

up to 99.5% after 4 h operation, better than the 1T-$MoSe_2$/TiC-C electrode (98.3%) and 2H-$MoSe_2$/TiC-C (99%), which reveals that the N-$MoSe_2$/TiC-C arrays possess the most stable life span with excellent large-current catalytic activity over long-time testing. In addition, similar cycling results are demonstrated at the low current density of 10 mA cm^{-2} (**Figure S7**a). SEM-TEM images and XRD result after 4h-HER test demonstrate that the phase and core/shell morphology of the N-MoSe2/TiC-C arrays are still well maintained (**Figure S8**), further revealing their excellent cycling stability. In addition, the Faradic efficiency was estimated by comparing the experimentally produced gas volume with the theoretically calculated one. **Figure S9** displays that the amount of evolved H_2 is in good agreement with the calculated value, suggesting a Faradic efficiency of about 100%. To further deepen the understanding of the improved HER performance of the N-$MoSe_2$/TiC-C electrode, the effective electrochemical active surface areas (ECSA) of all samples were estimated by testing the double-layer capacitance (Cdl) based on the CV results at different scan rates (**Figure S10**).[35, 36] The obtained current density is plotted as a function with scan rates in the **Figure 4**e. Noticeably, the ECSA of N-$MoSe_2$/TiC-C electrode is up to 57 mF cm^{-2}, substantially larger than the TiC-C (0.5 mF cm^{-2}), 1T-$MoSe_2$/TiC-C (47 mF cm^{-2}) and 2H-$MoSe_2$/TiC-C (12 mF cm^{-2}) electrodes, indicating the N doping can enhance the electrochemical active area and render more exposed active sites for catalysis. EIS tests were

carried out to additionally investigate electrochemical reaction kinetics during the HER process. The semicircle shown in Nyquist plot (**Figure 4**f) indicates the charge transfer resistance (R_{ct}) of H^+ reaction between electrode and electrolyte. Spectacularly, both the N-$MoSe_2$/TiC-C and 1T-$MoSe_2$/TiC-C electrodes only present a slope without obviously depressed semicircles compared to the TiC-C and 2H-$MoSe_2$/TiC-C electrodes, suggesting the fast hydrogen evolution reaction. In contrast, the depressed semicircles for the TiC-C and 2H-$MoSe_2$/TiC-C electrodes are much bigger, suggesting their slow HER process. Furthermore, the solution resistance (R_s) of sample is small due to the highly conductive TiC-C skeleton arrays. It is noteworthy that highly conductive TiC-C backbone can decrease the solution resistance, but itself with poor HER performance leading to high R_{ct} value for HER. But the N-$MoSe_2$/TiC-C electrode still exhibits the smallest solution resistance (1.12 Ω), suggesting that the introduction of N dopant can improve the electronic conductivity. Meanwhile, kinetic energy barrier and pathway of the HER activity on $MoSe_2$ surface are also important parameters to explain the surface performance of $MoSe_2$.[43] In order to check whether N doping can help to improve the HER activity, we also used the nudged elastic band method to study the process of HER on the surfaces of 2H-$MoSe_2$, 1T-$MoSe_2$, and N-$MoSe_2$, respectively. As shown in **Figure 5**, the process mainly involves hydrogen atom adsorption reaction and following formation and release of H_2.[44] From our calculations

(**Figure 5**), the energy barrier of two hydrogen atoms absorbed on the 2H-$MoSe_2$, 1T-$MoSe_2$, and N-$MoSe_2$ to transform into a H_2 molecule is gradually reduced, from 1.10 eV, 0.66 eV to 0.42 eV. On the other hand, when H_2 formed and released, the N-$MoSe_2$ electrode has better thermodynamic stability than the 2H-$MoSe_2$ and 1T-$MoSe_2$ electrode. The shortest bond lengths of H-Se are 1.49 Å, 1.58 Å, and 1.74 Å on 2H-MoSe, 1T-$MoSe_2$, and N-doped 2H-$MoSe_2$, respectively. Since the bond length is inversely proportional with H-Se bond strength, this indicates hydrogen atoms desorb easier from Se atom in N-$MoSe_2$/TiC-C sample and form H_2 molecule more effectively. Although 1T-$MoSe_2$ exhibits more suitable kinetic energy barrier for HER than 2H-$MoSe_2$, N-$MoSe_2$ still shows better HER performance than 1T-$MoSe_2$ promoting H_2 formation.

In summary, we have constructed high-quality N-$MoSe_2$/TiC-C shell/core arrays by morphological engineering in combination with nitrogen doping. Compared to other counterparts (1T-$MoSe_2$ and 2H-$MoSe_2$), the N-$MoSe_2$/TiC-C arrays with coexisted 1T- and 2H-$MoSe_2$ show improved electrochemical active surface area and much reduced charge transfer resistance and therefore boosted catalytic reaction sites and reaction kinetics. DFT calculation unravels much smaller energy barrier, longer H-Se bond length and diminished bandgap in N-$MoSe_2$/TiC-C arrays in terms of promoting H_2 formation, suggesting quasi-metallic nature of the material during phase transition upon N-doping demonstrated by

SACTEM. Consequently, the designed N-$MoSe_2$/TiC-C arrays exhibit extraordinary HER performance at large current density (i.e. 100 mA cm^{-2}) and low Tafel slope of 32 mV per decade, much more superior than other Mo-based compounds and even noble metal catalyst such as Pt/C. Remarkable potential retention as high as 99.5% under large current density of 100 mA cm^{-2} during 4 h-HER process is also able to be achieved, demonstrating excellent electrochemical stability of our designed nanoarchitecture.

Our work, for the first time, clearly demonstrates the phase change from 2H-$MoSe_2$ to 1T-$MoSe_2$ via NH_3 treatment and verifies the coexistence of 1T-$MoSe_2$ and 2H-$MoSe_2$ in the N-doped $MoSe_2$ by SACTEM. In addition, we first propose the plausible phase transformation mechanism (1T $\rightarrow$ 2H $\rightarrow$ 1T-2H) and different doping sites of N atom with the help of DFT calculation. Our research provides valuable reference to understand phase transformation mechanism of 2D transition metal dichalcogenides (TMDs) via hetero-atom doping, and also opens a new door to deeply understand the enhanced HER activity of metal selenides by nitrogen doping.

Supporting Information

Supporting Information is available from the Wiley Online Library or from the author.

Acknowledgements

This work is supported by National Natural Science Foundation of China (Grant No. 51728204, 51772272, 51502263 and 51462008), Fundamental Research Funds for the Central Universities (Grant No. 2018QNA4011), Qianjiang Talents Plan D (QJD1602029), Startup Foundation for Hundred-Talent Program of Zhejiang University, and the Fundamental Research Funds for the Central Universities (2015XZZX010-02), Key Research and Development Program of Hainan Province (ZDYF2017166). Guangdong Natural Science Funds for Distinguished Young Scholar (2014A030306048), and Pearl River S&T Nova Program of Guangzhou (201610010080). Work at Ames Laboratory was supported by the US Department of Energy, Basic Energy Sciences, Division of Materials Science and Engineering under Contract No. DE-AC02-07CH11358.

References

[1] T. Ling, D.-Y. Yan, H. Wang, Y. Jiao, Z. Hu, Y. Zheng, L. Zheng, J. Mao, H. Liu, X.-W. Du, Nat. Commun. 2017, 8, 1509.

[2] Q. Gong, L. Cheng, C. Liu, M. Zhang, Q. Feng, H. Ye, M. Zeng, L. Xie, Z. Liu, Y. Li, ACS Catalysis 2015, 5, 2213.

[3] J. Shi, X. Wang, S. Zhang, L. Xiao, Y. Huan, Y. Gong, Z. Zhang, Y. Li, X. Zhou, M. Hong, Nat. Commun. 2017, 8, 958.

[4] L. Yang, X. Li, G. Zhang, P. Cui, X. Wang, X. Jiang, J. Zhao, Y. Luo, J. Jiang, Nat. Commun. 2017, 8, 16049.

[5] J. J. Yan, Y. F. Zhang, Y. P. Huang, Y. E. Miao, T. X. Liu, Adv. Mater. Inter. 2017, 4.

[6] Y. Huang, H. Lu, H. Gu, J. Fu, S. Mo, C. Wei, Y.-E. Miao, T. Liu, Nanoscale 2015, 7, 18595.

[7] H. Li, S. Chen, X. Jia, B. Xu, H. Lin, H. Yang, L. Song, X. Wang, Nat. Commun. 2017, 8, 15377.

[8] K. Zhang, C. Li, Y. Zhao, X. Yu, Y. Chen, Phys. Chem. Chem. Phys. 2015, 17, 16609.

[9] K. Zhang, Y. Zhao, S. Zhang, H. Yu, Y. Chen, P. Gao, C. Zhu, J. Mater. Chem.A 2014, 2, 18715.

[10]C. Tang, H. S. Wang, H. F. Wang, Q. Zhang, G. L. Tian, J. Q. Nie, F. Wei, Adv. Mater. 2015, 27, 4516.

[11]S. J. Deng, Y. Zhong, Y. X. Zeng, Y. D. Wang, Z. J. Yao, F. Yang, S. W. Lin, X. L. Wang, X. H. Lu, X. H. Xia, J. P. Tu, Adv. Mater. 2017, 29, 1700748.

[12]J. Y. Zhang, T. T. Wang, P. T. Liu, Y. G. Liu, J. Ma, D. Q. Gao, Electrochim. Acta 2016, 217, 181.

[13]J. Yan, Y. Zhang, Y. Huang, Y. E. Miao, T. Liu, Adv. Mater. Inter. 2017, 4, 1600825.

[14]Z. Lei, S. Xu, P. Wu, Phys. Chem. Chem. Phys. 2016, 18, 70.

[15]M. Jiang, J. J. Zhang, M. H. Wu, W. J. Jian, H. T. Xue, T. W. Ng, C. S. Lee, J. Xu, J. Mater. Chem.A 2016, 4, 14949.

[16]Y. Yin, Y. M. Zhang, T. L. Gao, T. Yao, X. H. Zhang, J. C. Han, X. J. Wang, Z. H. Zhang, P. Xu, P. Zhang, X. Z. Cao, B. Song, S. Jin, Adv. Mater. 2017, 29.

[17]Y. Qu, H. Medina, S. W. Wang, Y. C. Wang, C. W. Chen, T. Y. Su, A. Manikandan, K. Wang, Y. C. Shih, J. W. Chang, Adv. Mater. 2016, 28, 9831.

[18]H. T. Wang, D. S. Kong, P. Johanes, J. J. Cha, G. Y. Zheng, K. Yan, N. A. Liu, Y. Cui, Nano Lett. 2013, 13, 3426.

[19]S. Deng, Y. Zhong, Y. Zeng, Y. Wang, X. Wang, X. Lu, X. Xia, J. Tu, Adv. Sci. 2017.

[20]D. Sun, S. Feng, M. Terrones, R. E. Schaak, Chem. Mater. 2015, 27, 3167.

[21]W. Guo, Y. Chen, L. Wang, J. Xu, D. Zeng, D.-L. Peng, Electrochim. Acta 2017, 231, 69.

[22]C. Dai, Z. Zhou, C. Tian, Y. Li, C. Yang, X. Gao, X. Tian, J. Phys. Chem. C 2017, 121, 1974.

[23]S. Mao, Z. Wen, S. Ci, X. Guo, K. K. Ostrikov, J. Chen, Small 2015, 11, 414.

[24]Y. Liu, L. Ren, Z. Zhang, X. Qi, H. Li, J. Zhong, Sci. Rep. 2016, 6, 22516.

[25]G. D. Park, J. H. Kim, S.-K. Park, Y. C. Kang, ACS Appl. Mater. Interfaces 2017, 9, 10673.

[26]Y. Yao, K. Huo, L. Hu, N. Liu, J. J. Cha, M. T. Mcdowell, P. K. Chu, Y. Cui, ACS Nano 2011, 5, 8346.

[27]S. Liu, X. Xia, Y. Zhong, S. Deng, Z. Yao, L. Zhang, X. B. Cheng, X. Wang, Q. Zhang, J. Tu, Adv. Energy Mater. 2017, 1702322.

[28]M. Jiang, J. Zhang, M. Wu, W. Jian, H. Xue, T.-W. Ng, C.-S. Lee, J. Xu, J. Mater. Chem.A 2016, 4, 14949.

[29]J. Zhang, T. Wang, P. Liu, Y. Liu, J. Ma, D. Gao, Electrochim. Acta 2016, 217, 181.

[30]C. Tan, X. Cao, X.-J. Wu, Q. He, J. Yang, X. Zhang, J. Chen, W. Zhao, S. Han, G.-H. Nam, Chem. Rev. 2017, 117, 6225.

[31]D. Voiry, A. Goswami, R. Kappera, C. d. C. C. e Silva, D. Kaplan, T. Fujita, M. Chen, T. Asefa, M. Chhowalla, Nature chemistry 2015, 7, 45.

[32]N. Rohaizad, C. C. Mayorga-Martinez, Z. k. Sofer, M. Pumera, ACS Appl. Mater. Interfaces 2017, 9, 40697.

[33]K. Inumaru, K. Baba, S. Yamanaka, Physica B: Condensed Matter 2006, 383, 84.

[34]P. Liu, Y. Liu, W. Ye, J. Ma, D. Gao, Nanotechnology 2016, 27, 225403.

[35]Y. Zhang, B. Ouyang, J. Xu, G. Jia, S. Chen, R. S. Rawat, H. J. Fan, Angew. Chem. Int. Ed. 2016, 55, 8670.

[36]J. W. Huang, H. Q. Liu, B. Jin, M. Liu, Q. C. Zhang, L. Q. Luo, S. J. Chu, S. Chu, R. F. Peng, Nanotechnology 2017, 28.

[37]H. Tang, K. Dou, C.-C. Kaun, Q. Kuang, S. Yang, J. Mater. Chem.A 2014, 2, 360.

[38]K. Zhang, Y. Zhao, D. Fu, Y. Chen, J. Mater. Chem.A 2015, 3, 5783.

[39]B. Qu, X. Yu, Y. Chen, C. Zhu, C. Li, Z. Yin, X. Zhang, ACS Appl. Mater. Interfaces 2015, 7, 14170.

[40]B. Qu, C. Li, C. Zhu, S. Wang, X. Zhang, Y. Chen, Nanoscale 2016, 8, 16886.

[41]Y. Huang, Y.-E. Miao, L. Zhang, W. W. Tjiu, J. Pan, T. Liu, Nanoscale 2014, 6, 10673.

[42]C. Xu, S. Peng, C. Tan, H. Ang, H. Tan, H. Zhang, Q. Yan, J. Mater. Chem.A 2014, 2, 5597.

[43]E. Skúlason, G. S. Karlberg, J. Rossmeisl, T. Bligaard, J. Greeley, H. Jónsson, J. K. Nørskov, Phys. Chem. Chem. Phys. 2007, 9, 3241.

[44]D.-Y. Wang, M. Gong, H.-L. Chou, C.-J. Pan, H.-A. Chen, Y. Wu, M.-C. Lin, M. Guan, J. Yang, C.-W. Chen, J. Am. Chem. Soc. 2015, 137, 1587.

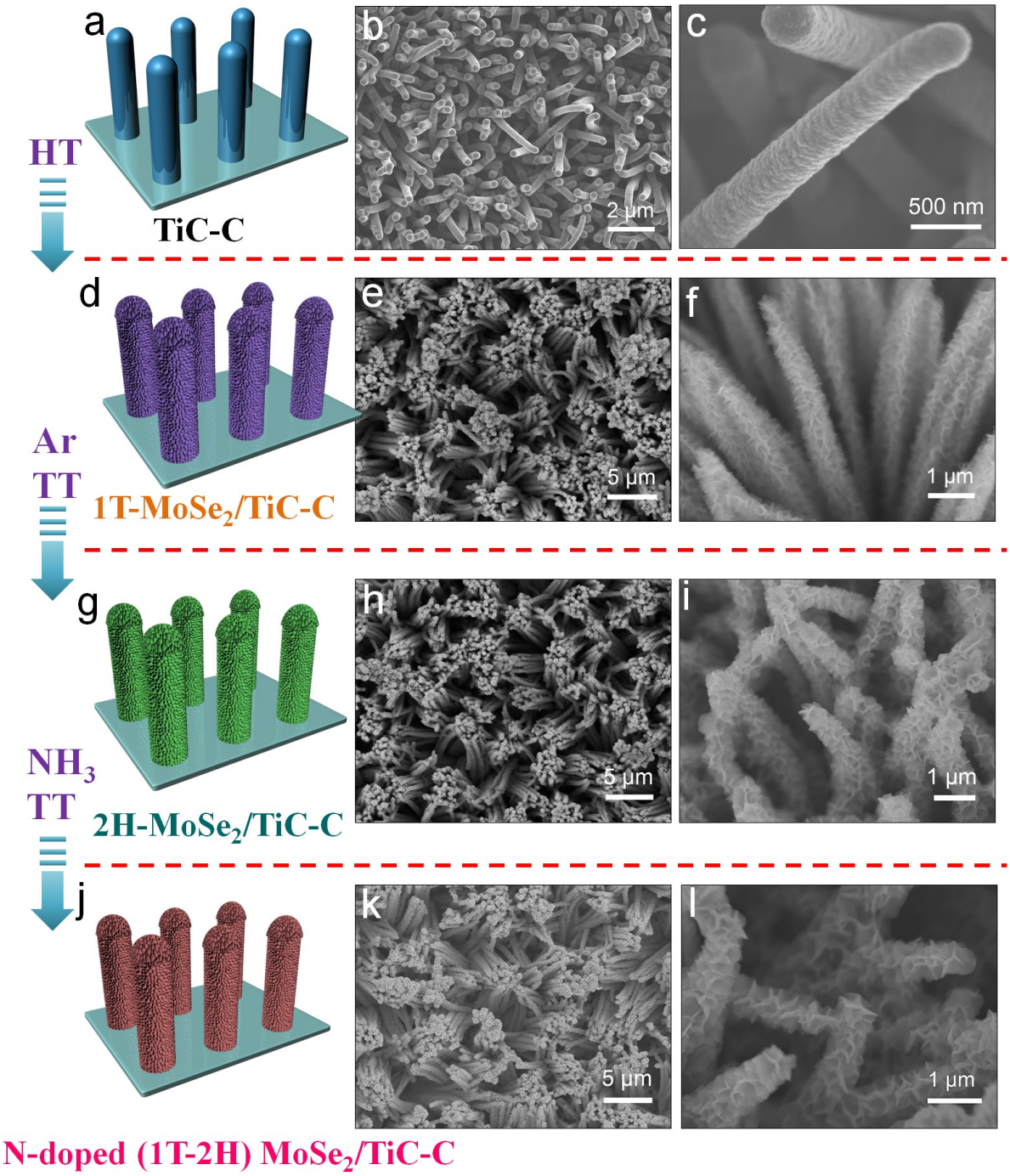

Figure 1. (a, d, g, j) Schematic illustration of the synthesis of N-$MoSe_2$/TiC-C arrays. SEM images of (b, c) TiC-C arrays; (e, f) 1T-$MoSe_2$/TiC-C arrays; (h, i) 2H-$MoSe_2$/TiC-C arrays and (k, l) N-$MoSe_2$/TiC-C arrays.

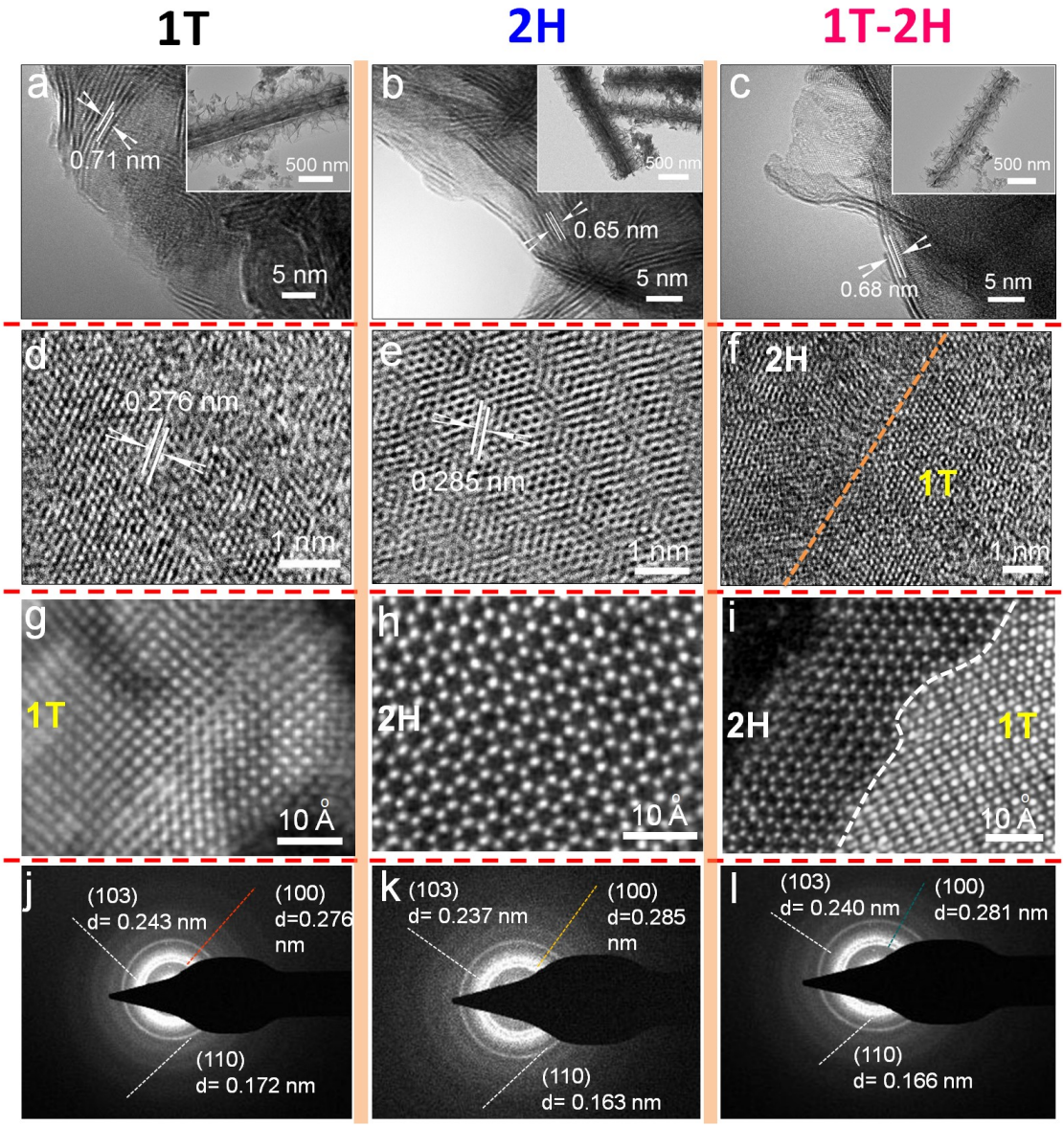

Figure 2. TEM-HRTEM images and SAED patterns of different $MoSe_2$ nanosheets: (a, d, g, h) 1T-$MoSe_2$/TiC-C; (b, e, h, k) 2H-$MoSe_2$/TiC-C and (c, f, i, l) N-$MoSe_2$/TiC-C samples. (SACTEM images: g-1T; h-2H; i-1T-2H)

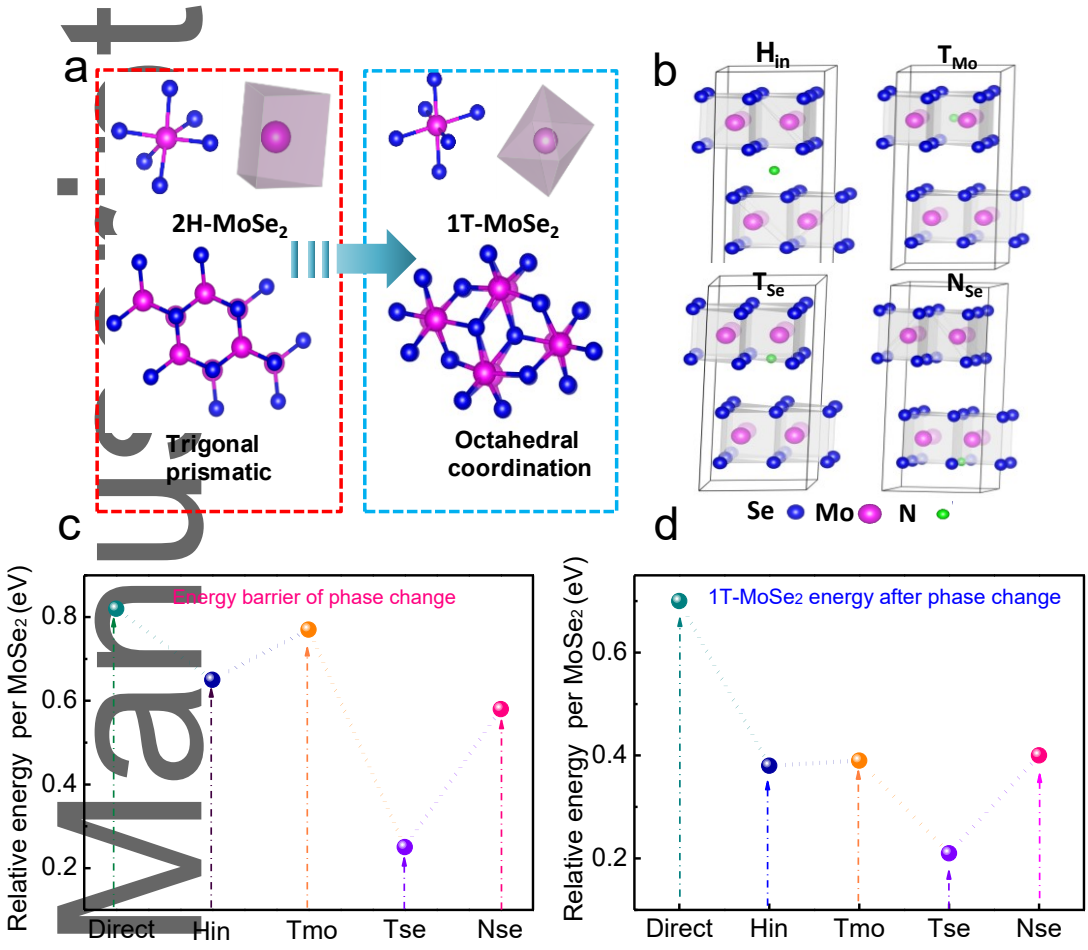

Figure 3. (a) Schematic crystal structures of 2H-$MoSe_2$ and 1T-$MoSe_2$; Schematic representations of the N dopant at the H_{in} site, T_{Mo} site, T_{Se} site, and substitution site (N_{Se}), respectively; (c) Kinetic energy barrier of phase transition from 2H-$MoSe_2$ to 1T-$MoSe_2$ by N doping at different sites; (d) Energy of 1T-$MoSe_2$ obtained after phase change with different N sites.

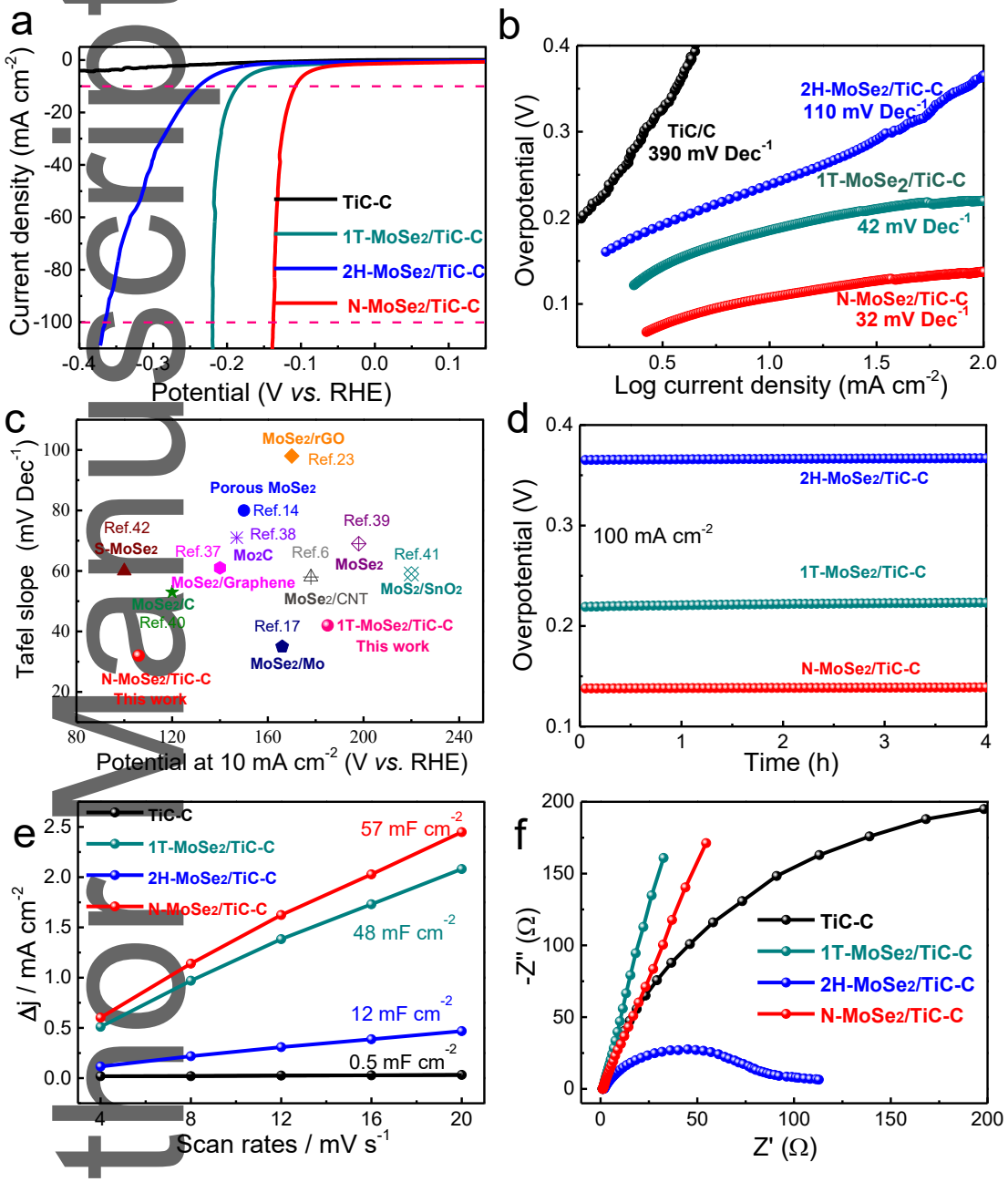

Figure 4. (a) LSV curves and (b) Tafel plots of the TiC-C, 1T-$MoSe_2$/TiC-C, 2H-$MoSe_2$/TiC-C and N-$MoSe_2$/TiC-C electrodes. (c) HER performance comparison of different Mo-based materials; (d) Electrochemical stability of the 1T-$MoSe_2$/TiC-C, 2H-$MoSe_2$/TiC-C and N-$MoSe_2$/TiC-C electrodes. (e) The ratio of current density with various scan rates and (f) Nyquist plots of all samples.

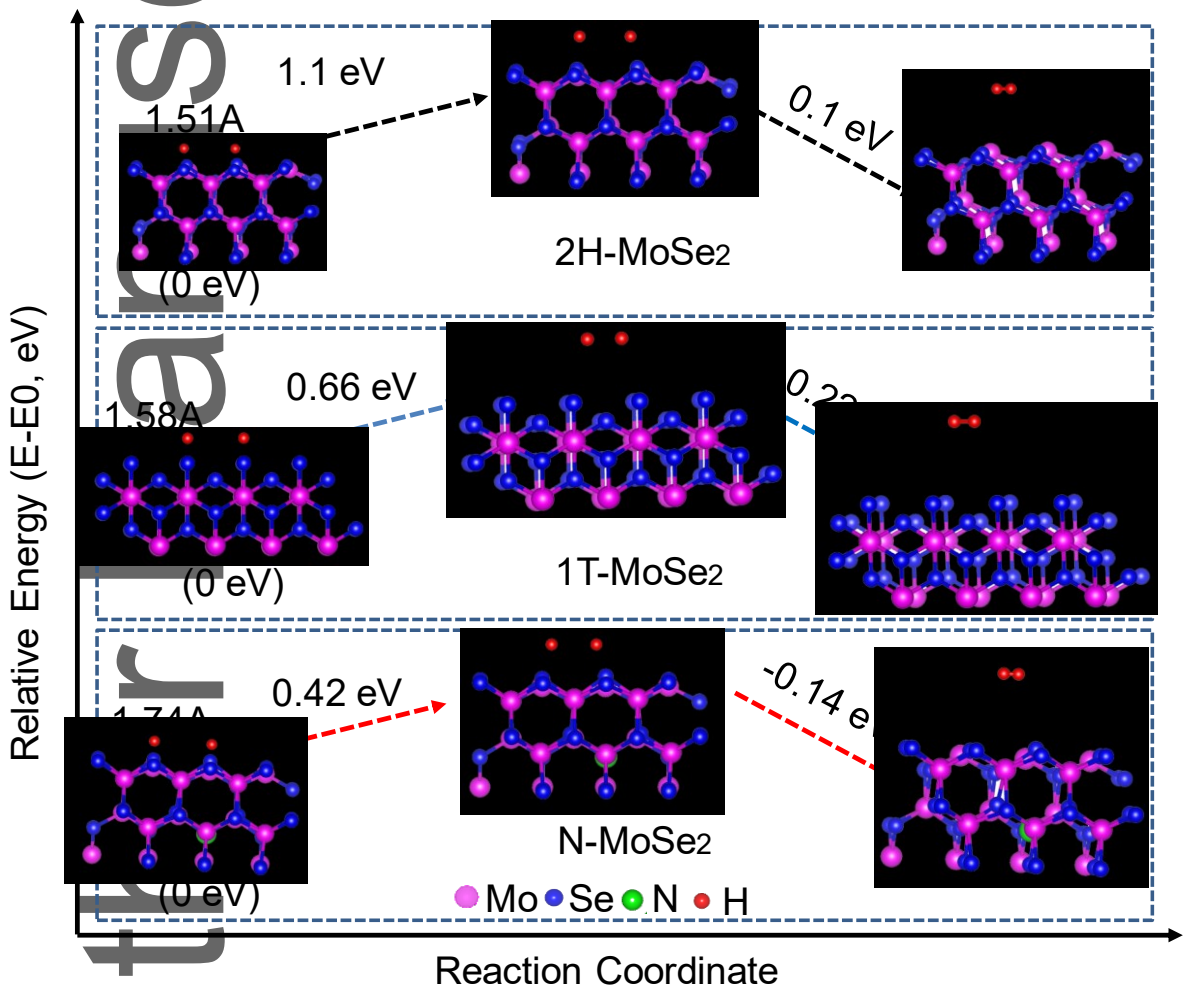

Figure 5. Calculated potential barriers of hydrogen evolution reaction on 2H-$MoSe_2$, 1T-$MoSe_2$, and N-$MoSe_2$ samples.

Keywords: Molybdenum selenide; Nitrogen doping; Phase modulation; Hydrogen evolution reaction; Core/shell arrays

Shengjue Deng‡, Fan Yang‡, Qinghua Zhang, Yu Zhong, Yinxiang Zeng, Shiwei Lin, Xiuli Wang, Xihong Lu*, Cai-Zhuang Wang, Lin Gu, Xinhui Xia* and Jiangping Tu*

Phase Modulation of (1T-2H)-$MoSe_2$/TiC-C Shell/Core Arrays via Nitrogen Doping for Highly Efficient Hydrogen Evolution Reaction

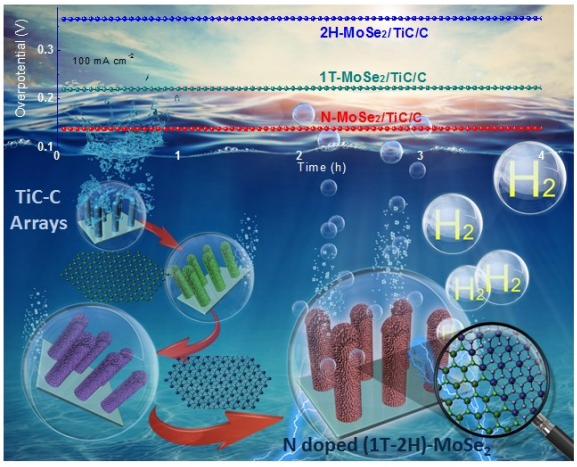

In this work, we report phase- and morphology-modulated N-doped $MoSe_2$/TiC-C shell/core arrays for the first time. We successfully realize the continuous phase modulation of $MoSe_2$ (1T $\rightarrow$ 2H $\rightarrow$ 1T-2H) on the TiC-C skeleton via NH_3 treatment and demonstrated by spherical aberration electron microscope. In addition, we first propose the plausible phase transformation mechanism (1T $\rightarrow$ 2H $\rightarrow$ 1T-2H) and different doping sites of N atom with the help of DFT calculation. The designed N-$MoSe_2$/TiC-C arrays exhibit extraordinary HER performance.